https://doi.org/10.1016/j.apenergy.2019.02.068

Title: A novel 3D simulation model for investigating liquid desiccant dehumidification performance based on CFD technology

Author: Wen Tao[1], Luo Yimo[2], Lu Lin[1,*] (vivien.lu@polyu.edu.hk)

[1]Department of Building Services Engineering, The Hong Kong Polytechnic University, Hong Kong, China

[2]Faculty of Science and Technology, Technological and Higher Education Institute of Hong Kong, Hong Kong, China

Abstract: Previous 2D CFD simulation models fail to elaborate the actual simultaneous flow and dehumidification process in liquid desiccant cooling system. Accordingly, the present study successfully developed a novel 3D simulation model for investigating the liquid desiccant dehumidification performance of a falling film dehumidifier. The penetration mass transfer model was implemented in the simulation to account for the interfacial dehumidification process. Experimental system was built for the model validation and the results indicated that the newly developed 3D CFD model could predict the absolute moisture removal accurately with an average deviation of 7%. Parametric study revealed that the dehumidification performance was closely related with air humidity, velocity, solution temperature, centration, temperature and contact angle but seldom affected by air temperature. The simulation results also indicated that falling film of liquid desiccant shrank gradually along the flow direction, leading to an inhomogeneous water vapor absorption process in the dehumidifier. Intense water vapor absorption occurred at the phase interface, resulting in large solution concentration gradient and humidity content in the zone near the air/liquid contact interface. However, minor mass transfer occurred in other zones mainly in the form of diffusion. Accordingly, several heat/mass transfer enhancement approaches, i.e. structural modifications and surface modification, were proposed to improve the flow turbulence and to enlarge the falling film wettability. The newly proposed 3D simulation model and dehumidification enhancement approaches are meaningful for the design and operation of liquid desiccant cooling system.

Key words: falling film dehumidification; film shrinkage; contact angle; penetration theory; 3D CFD simulation

Nomenclature			
A	Mass transfer area (m^2)	t_c	Contact time (s)
c_p	Specific heat (J/(kg.K))	T	Temperature ($^{\circ}C$)
$C_{1\varepsilon}$, $C_{2\varepsilon}$	Constants	u_{surf}	Surface velocity of liquid film (m/s)
d	Absolute humidity (g/kg)	u	Velocity (m/s)
D	Diffusion coefficient (m^2/s)	x	x direction
E	Energy(J/kg)	X	Concentration (%)
$\vec{F}$	Momentum source term (N/m^3)	y	y direction
g	gravitational acceleration (m/s^2)	z	z direction
G	Mass flow rate (kg/s)	Greek symbols	
h	Enthalpy (J/kg)	α	The volume fraction of phase
h_m	Local mass transfer coefficient (kg/(m^2.s))	μ	Dynamic viscosity (Pa.s)
H_{lg}	Latent heat of evaporation (J/kg)	υ	Kinetic viscosity (m^2/s)
k	Thermal conductivity (W/(m.K)) Turbulence kinetic energy (m^2/s)	ρ	Density (kg/m^3)
K	Overall mass transfer coefficient (kg/(m^2.s))	ψ	Concentration difference ratio
l	Flow distance (m)	Subscripts	
$LDCS$	Liquid desiccant cooling system	g	Gas phase
m	The number of species	e	Equilibrium
n	The number of phases	m	Main part
p	Pressure (Pa)	r	Rim part
S_E	Energy source term (W/m^3)	s	Solution
S_{lg}	Mass transfer source term (kg/m^3)		

1 Introduction

To keep a livable and comfortable indoor environmental for residents, it is essential to adjust the indoor temperature and humidity to a desirable degree [1, 2]. In nowadays, the vapor compression cooling system (VCS) is used worldwide to achieve such goal [3]. In the VCS, the sensible and latent heat loads which correspond to temperature and humidity control are dealt with by cooling the processed air under its dew point temperature. However, in order to get satisfactory temperature for supply air, reheating is required in some situations, which is a kind of energy waste [4-6]. Moreover, the VCS has been criticized by its heavy reliance on electricity consumption. In order to avoid the reheating and improve the system efficiency, the sensible and latent heat loads are supposed to be handled with separately [7, 8]. For the sensible load, it can be removed by a cooling coil and for the latent load in the

form of extra water vapor in processed air, it can be dealt with by various approaches, such as electrochemical dehumidification, liquid desiccant dehumidification and solid desiccant dehumidification [9, 10]. Among all these approaches, the liquid desiccant dehumidification has drawn increasing attention in the last few decades due to its accurate control ability of humidity and great energy saving potential. Different from the conventional VCS, the liquid desiccant cooling system (LDCS) can utilize low grade or renewable energy sources, such as geothermal energy, waste heat and solar thermal energy, which helps to significantly improve the system efficiency [11, 12]. Moreover, the LDCS has the potential of energy conservation up to 30~50% compared with the conventional VCS [13].

A schematic diagram of a liquid desiccant dehumidification process is shown in Fig. 1. Liquid desiccant, such as lithium bromide (LiBr) and lithium chloride (LiCl) solution, with low temperature and high concentration gets in contact with processed moist air in a dehumidifier. Driven by the vapor pressure difference between desiccant solution and processed air, water vapor in the air would be absorbed by the liquid desiccant to achieve the purpose of dehumidification. After that, solution will be regenerated in a regeneration for continuous system operation. In order to uncover the heat and mass transfer characteristics in the dehumidifier/regenerator, plenty of researches have been carried out [14-19]. Generally speaking, these researches can be divided into two groups: experimental investigation [14-17] and numerical study [18-20]. Even though experimental study can provide intuitional data for practical application, the cost in terms of money and time is usually high. Therefore, a lot of researchers choose to numerically investigate the dehumidification/regeneration performance in the LDCS. Benefiting from the development of computer science, it is able to use the computational fluid dynamic (CFD) technology to analyze the detailed and complicated fluid flow and heat transfer process [21]. In fact, the CFD method has shown its convenience and superiority in various fields, such as chemical reaction, aircraft design and fluid dynamics [22-24], and will become more and more popular in the foreseeable future.

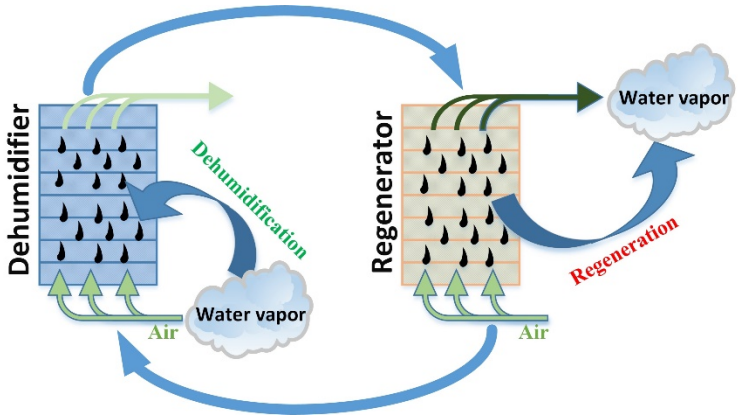

Fig. 1. Schematic diagram of liquid desiccant dehumidification.

In the field of mass transfer concerning absorption or dehumidification, there are some researches on the investigation of hydrodynamics characteristics and simultaneous heat and mass transfer [20-30]. As the falling film flow on plate or packing material is the typical flow pattern during absorption or dehumidification, some studies focused on simulating the hydrodynamics characteristics of the falling film. Min et al. [25] studied the motions of laminar wavy film flow on a vertical plate by CFD simulation. VOF and PLIC methods were used to capture the interface between liquid and gas. The simulation results showed good agreement with the experimental ones in respect of wave shape as well as wave motion. Differently, Gu et al. [26] studied the hydrodynamics of falling film on an inclined flat plate and a wavy plate by their developed two-dimensional (2D) CFD model. Besides, Szulczewska et al. [27] and Ho et al. [28] also numerically investigated the hydrodynamics characteristics of falling film on different kinds of plates. Compared with the 2D simulation, 3D simulation can get more actual flow characteristics of both gas and liquid. Ho et al. [28] also conducted the 3D simulation to study the falling film behavior of a micro-reactor. Their results indicated that velocity profiles in the liquid film and near-liquid gas zone were complex and was not consistent with the conventional simplified assumptions. Subramanian et al. [29] carried out 3D simulation to study the falling film flow of different fluids on corrugated sheets of packing. The wettability, film thickness and flow dynamics of falling film were obtained through simulation and shown good agreement with experiments. Xu et al. [30] investigated the flow behavior of a liquid phase flowing on an inclined steel plate

at different situations with the consideration of drag force between gas phase and liquid phase. With the developed 3D model, the influences of the liquid and gas flow rate on wetted area, the characteristics of film thickness and velocity profiles were studied. However, the abovementioned studies only cared about the hydrodynamics characteristics of falling film while did not concern the heat and mass transfer process. In fact, when taking the heat and mass transfer into consideration, the simulation becomes complex and cannot be completed only by the internal code of CFD commercial software (such as Fluent and CFX). With the help of User Defined Function (UDF), external govern equations can be jointly solved with the internal code to get the thermal, flow and concentration profiles.

Some studies concerning the ethanol evaporation [31], LiBr solution absorption [32] and water evaporation [33] of falling film on plates have been carried out by previous researchers. In these studies, the VOF model was widely used to track the interface between liquid phase and gas phase. The interfacial heat and mass transfer characteristics were determined by the UDF code coupled into the Fluent solver. Bo et al. [34] conducted a 2D simulation to investigate the falling film absorption of LiBr solution in a counter-flow absorber. The interfacial heat flux was determined by the Fickian law of diffusion. Based on the developed model, the detailed heat and mass transfer process during absorption was analyzed. Kharangate et al. [33] proposed a 2D CFD model to predict the heat and mass transfer behavior of evaporative falling films on plate. Based on phase change model, heat and mass source terms were coupled into the solver in the form of UDF. Results indicated that the model successfully predicted the evaporation and flow behavior characteristics in a broad range of Reynolds number. Based on the 2D CFD simulation model, Hu et al. [35] paid their attention on the CO_2 absorption by a confined falling film. According to the simulation results, the mechanism of mass transfer and relationship between mass transfer and flow behavior were explored and discussed. Based on the commercial CFD software of Fluent, Haelssig et al [36] conducted a direct numerical simulation to analyze the dynamics and simultaneous heat and mass transfer process of phase interface in a system with multiple chemical species. Good agreement between experimental data and numerical

prediction was observed.

Regarding liquid desiccant, only few researches were reported which will be elaborately discussed below. Luo et al. [7] firstly conducted the dynamic and microscopic simulation to study the flow mechanism of LiCl solution on plate dehumidifier. The influences of different parameters on velocity field, wettability, minimum wetting ratio and film thickness were identified. Later, they simultaneously simulated the heat and mass transfer performance in a LiCl solution based falling film dehumidifier [37]. The penetration mass transfer theory was adopted to describe the dynamic dehumidification process at the interface of liquid desiccant and processed air. The developed model was proved to be reliable by comparing the simulation results with other models, and parametric studies were conducted to investigate the effects of different boundary conditions. Furthermore, Luo et al. [38] developed a 2D CFD simulation model for an internal cooling dehumidifier. By adopting the developed model, analysis was carried out to identify the influences of solution temperature, flow rate and different types of internal cooling modes on dehumidification performance. As one can see, the CFD technology can not only predict the hydrodynamic behavior of fluid flow but also simultaneous heat and mass transfer process in various areas which include absorption refrigeration, evaporative cooling, condensation and various chemical processes. In nowadays, it is not just a supplement or substitution of experimental study. It becomes an indispensable approach to get the detailed information on local heat and mass transfer behavior. Such information is of vital importance to explore the transfer mechanism and develop related correlations for practical applications. However, for simulation integrated with mass transfer, as there is no existing mass transfer model in the CFD software, investigators have to develop corresponding models for different situations. In addition, the large computational cost forces researchers to choose a high-performance computing device with high cost.

Regarding liquid desiccant falling film, the only reported CFD simulations were 2D [37-39]. However, the 2D simulation cannot evaluate the contraction of falling film which has been observed [40, 41], which significantly affects the heat and mass

transfer performance [42]. Therefore, it is better to conduct 3D simulation for the dehumidification process to uncover the simultaneous heat and mass transfer behavior. The present study newly developed a 3D simulation model for a falling film dehumidifier based on the CFD technology. An experimental system with a single channel dehumidifier was also fabricated for the validation of the developed 3D model. After the validation, parametric studies were carried out with the developed 3D model to analyze the influences of different parameters on dehumidification performance. Further, some practical suggestions for the improvement of dehumidification performance in terms of surface treatment by super-hydrophilic coating and structural modification were also newly put forward. For better understanding of present study, a flow chart shown in Fig. 2 is given.

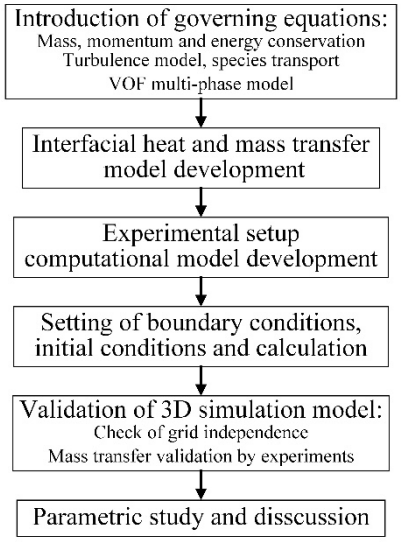

Fig. 2. Flow chart of present study.

2 Description of CFD model

2.1 Mathematical description of governing equations

In order to obtain the heat and mass transfer characteristics in the falling film dehumidifier, the mass conservation, energy conservation, momentum conservation and turbulence equations were solved by Fluent solver. The species transport equation was used to describe the mass transfer in the moist air and liquid desiccant. The Volume of Fraction (VOF) model was adopted to capture the phase interface between air and liquid desiccant. The formulations for them are detailed as follows:

(1) Mass conservation equation

$$\frac{\partial}{\partial t}(\rho)+\nabla\cdot\left(\rho\vec{u}\right)=0 \tag{1}$$

where ρ is the density and $\vec{u}$ is the vector of velocity.

(2) Energy conservation equation

$$\frac{\partial}{\partial t}(\rho E)+\nabla\cdot\left(\vec{u}(\rho E+P)\right)=\nabla\cdot\left[k_{\text{eff}}\nabla T-\sum h_{\text{k}}J_{\text{k}}\right]+S_{\text{E}} \tag{2}$$

where E means the energy and is defined by Equation (3). P and T are the pressure and absolute temperature. k_{eff} is the effective thermal conductivity and h and J are the enthalpy and diffusion flux of species. S_{E} represents the volumetric heat source.

$$E=h-\frac{P}{\rho}+\frac{u^2}{2} \tag{3}$$

(3) Momentum conservation equation

$$\frac{\partial}{\partial t}\left(\rho\vec{u}\right)+\nabla\cdot\left(\rho\vec{u}\vec{u}\right)=-\nabla P+\nabla\cdot(\mu(\nabla\vec{u}+\nabla\vec{u}^{T}))+\rho\vec{g}+\vec{F} \tag{4}$$

in which, μ is the viscosity and is $\vec{g}$ the acceleration of gravity. $\vec{F}$ Means the external body force or source term.

(4) Turbulence model

The Reynolds number of falling film is less than 400 and the value for processed air is in the range of 5800~13000 in this investigation. As a result, the flow patterns of processed air and liquid falling film are laminar flow and turbulent flow respectively. According to previous study [43], the $k-\varepsilon$ and k-ω model are usually adopted for the problem of falling film stratified two-phase flow. The RNG (Renormalization group) $k-\varepsilon$ model is the most adopted one. Banerjee and Isaac [44] compared the commonly used turbulence model of standard $k-\varepsilon$ model, RNG $k-\varepsilon$ model and RSM model for the stratified two-phase flow. Their results shown that the RNG $k-\varepsilon$ model gave the best prediction of experimental results. Moreover, as the Reynolds number of present study is not very high, the RNG $k-\varepsilon$ model is suitable according to the Users Guide of Fluent [45]. Based on the above references and Users Guide, the RNG $k-\varepsilon$ turbulence model was selected to describe the hydrodynamics

behavior in the dehumidifier. The governing equations of turbulence kinetic energy and its dissipation rate are gives as follows,

$$\frac{\partial}{\partial t}(\rho k)+\frac{\partial}{\partial x_{\mathrm{i}}}(\rho k u_{\mathrm{i}})=\frac{\partial}{\partial x_{\mathrm{j}}}(\alpha_{\mathrm{k}}\mu_{\mathrm{eff}}\frac{\partial k}{\partial x_{\mathrm{j}}})+G_{\mathrm{k}}+G_{\mathrm{b}}-\rho\varepsilon-Y_{\mathrm{M}}+S_{\mathrm{k}} \tag{5}$$

$$\frac{\partial}{\partial t}(\rho\varepsilon)+\frac{\partial}{\partial x_{\mathrm{i}}}(\rho\varepsilon u_{\mathrm{i}})=\frac{\partial}{\partial x_{\mathrm{j}}}(\alpha_{\varepsilon}\mu_{\mathrm{eff}}\frac{\partial\varepsilon}{\partial x_{\mathrm{j}}})+C_{1\varepsilon}\frac{\varepsilon}{k}(G_{\mathrm{k}}+C_{3\varepsilon}G_{b})-C_{2\varepsilon}\rho\frac{\varepsilon^{2}}{k}-R_{\varepsilon}+S_{\varepsilon} \tag{6}$$

(5) Species transport equation

$$\frac{\partial}{\partial t}\left(\alpha_{\mathrm{q}}\rho_{\mathrm{q}}x_{\mathrm{k,q}}\right)+\nabla\cdot\left(\alpha_{\mathrm{q}}\rho_{\mathrm{q}}\vec{u}x_{\mathrm{k,q}}-\alpha_{\mathrm{q}}D_{\mathrm{k,q}}\nabla x_{\mathrm{k,q}}\right)=S_{\mathrm{lg,k}} \tag{7}$$

where $x_{\mathrm{k,q}}$ is the mass fraction of the k_{th} component in the corresponding phase q_{th}. $D_{\mathrm{k,q}}$ represents the coefficient of diffusion and $S_{\mathrm{lg,k}}$ stands for source term of mass transfer at the interface.

(6) VOF multi-phase model

The density and viscosity of each computational cell in the VOF model are described by Equation (8) and (9).

$$\rho=\alpha_{\mathrm{l}}\rho_{\mathrm{l}}+\alpha_{\mathrm{g}}\rho_{\mathrm{g}} \tag{8}$$

$$\mu=\alpha_{\mathrm{l}}\mu_{\mathrm{l}}+\alpha_{\mathrm{g}}\mu_{\mathrm{g}} \tag{9}$$

where α_{l} and α_{g} stand for the volume fraction of liquid phase and gas phase with the value ranging from 0 to 1. The value 1 for volume fraction means that the computational cell is filled with only one phase and the volume fraction for the other phase is 0, and vice versa. Obviously, the sum of the two volume fractions is equal to 1 as described in Equation (10).

$$\alpha_{\mathrm{g}}+\alpha_{\mathrm{l}}=1 \tag{10}$$

In order to track the interface between the gas phase and liquid phase, the continuity equation for volume fraction shown in Equation (11) is solved.

$$\frac{\partial\alpha_{\mathrm{l/g}}}{\partial t}+\vec{u}\cdot\nabla\alpha_{\mathrm{l/g}}=0 \tag{11}$$

2.2 Description of interface conditions

During the dehumidification process, water vapor at the phase interface is absorbed by the liquid desiccant due to vapor pressure difference. Simultaneously,

latent heat would also be released as vapor phase change occurs. Therefore, the mass and energy source terms need to be added into the species transport equation and energy conservation equation correspondingly. The calculation methods for the source terms are specified in the following part.

(1) Interface mass source

According to previous research, the mass transfer resistance at the phase interface is usually ignored [46]. Therefore, the overall mass transfer coefficient K is formulated in Equation (12) [47].

$$\frac{1}{K}=\frac{1}{h_{\mathrm{m,g}}}+\frac{1}{\psi h_{\mathrm{m,l}}} \tag{12}$$

where $h_{\mathrm{m,g}}$ and $h_{\mathrm{m,l}}$ stand for the local mass transfer coefficient of gas phase and liquid phase respectively. ψ is a factor related with the concentration and temperature of the liquid desiccant. The local mass transfer coefficient is determined according to the penetration mass transfer theory. The formulations for $h_{\mathrm{m,g}}$ and $h_{\mathrm{m,l}}$ are specified in Equation (13) and (14).

$$h_{\mathrm{m,g}}=2\sqrt{\frac{D_g}{\pi t_{\mathrm{c}}}} \tag{13}$$

$$h_{\mathrm{m,l}}=2\sqrt{\frac{D_{\mathrm{l}}}{\pi t_{\mathrm{c}}}} \tag{14}$$

where D_g and D_{l} are the diffusion coefficients of processed air and liquid desiccant respectively. t_{c} means the contact time between air and solution and is calculated by Equation (15),

$$t_{\mathrm{c}}=\frac{l}{u_{\mathrm{surf}}} \tag{15}$$

where l is the flow distance of the falling film and u_{surf} is the velocity of falling film which can be obtained by the cell macro supplied by Fluent software.

After the determination of overall mass transfer coefficient K, the mass source term $S_{\mathrm{lg,k}}$ in the species transport equation (7) can be obtained by Equation (16).

$$S_{\mathrm{lg,k}} = K(d_g - d_{\mathrm{e}})A \tag{16}$$

in which, d_g and d_e stand for the humidity of air and the equivalent air humidity of solution at its concentration and temperature. A represents the mass transfer contact area or the wetting area. It is worth noting that in the 2D model, the whole dehumidifier plate is assumed to be fully wetted by falling film. However, in 3D model, the film shrinkage can be simulated and only the actual wetted area takes part in the dehumidification process.

(2) Interface energy source

The latent heat of water vapor condensation and dilution heat of desiccant solution are generated during the process of dehumidification. As the dilution heat is much smaller that the condensation latent, it is neglected in the model [48]. As a result, the energy source term at the phase interface is calculated by Equation (17) as follows,

$$S_{\mathrm{E}} = \sum_{k=0}^{m-1} S_{\mathrm{lg,k}} H_{\mathrm{lg,k}} \tag{17}$$

By integrating the governing equations shown from Equation (1) to Equation (11) and the interface sources terms determined by Equation (16) and Equation (17), the comprehensive hydrodynamics and heat and mass transfer characteristics in a falling film dehumidifier can be obtained.

3 Experimental setup and model configuration

3.1 Introduction of experimental system

An experimental system was designed and built up to validate the 3D simulation model, as shown in Fig. 3. The whole system contained two subsystems, namely air subsystem and solution subsystem. A single channel falling film dehumidifier with the dimension of 500 mm×30 mm×540 mm (Length×Width×Height) was fabricated and installed in the system. As the liquid desiccant of LiCl solution is corrosive, the stainless steel of 316L with excellent corrosion resistance ability was used to be the material of the dehumidifier and plastic pipe was used for the solution loop. The whole system was covered by thermal insulation cotton to prevent the heat exchange between the whole system and ambient environment. It is noteworthy that the dimension of dehumidifier was determined according to dehumidification

performance and the whole size of the system. In order to get desirable dehumidification performance, the length and height of the dehumidifier are usually in the range of 200~700mm according to previous studies. Moreover, the whole system was installed in an air-conditioning system, the whole size of the experimental system was limited by the size of the air-conditioning room. Finally, after careful consideration and validation, we chose the dehumidifier with the size of 500 mm×30 mm×540 mm (Length×Width×Height).

The liquid desiccant was stored in one plastic tank before the experiment. An electrical heater controlled by a Proportion-Integration-Differentiation (PID) controller was used to heat the liquid desiccant to the desired temperature. Driven by a pump connected with the tank, the liquid desiccant circulated in the pipe and flowed through a three-way valve firstly. By adjusting the opening angle of this valve, the flow rate of solution could be changed and its exact value was measured by a turbine flow rate meter with a relative accuracy of $\pm 3\%$. A distributor shown in Fig. 3 was used to uniformly distribute the liquid desiccant on the plate. When the falling film flowed through the plate and got in contact with the processed air, it flowed back to another solution tank. The inlet and outlet solution temperatures were measured by two Pt-100 thermocouples with an accuracy of 0.1 K. The ambient air was blown into the air duct by a blower. There was a valve in the air duct to adjust the air flow rate. In order to get processed air with desired temperature and humidity, an electrical heater and a humidifier were installed at the inlet of the air duct. The values of air temperature and humidity at the inlet and outlet dehumidifier were obtained by two temperature and humidity sensors with the accuracy of 0.1 K for temperature and 2.5% for humidity. The air flow rate was measured by a micro-manometer and a pitot tube installed at the outlet of dehumidifier with a measurement accuracy of 2.2%. All of the signals generated by different sensors were collected, displayed and stored by a data logger during the experiments. It is worth noting that the experimental study was just to provide reliable validation data for the developed 3D CFD model. Therefore, we only emphasized our main work of CFD simulation in the title without mentioning the experimental work.

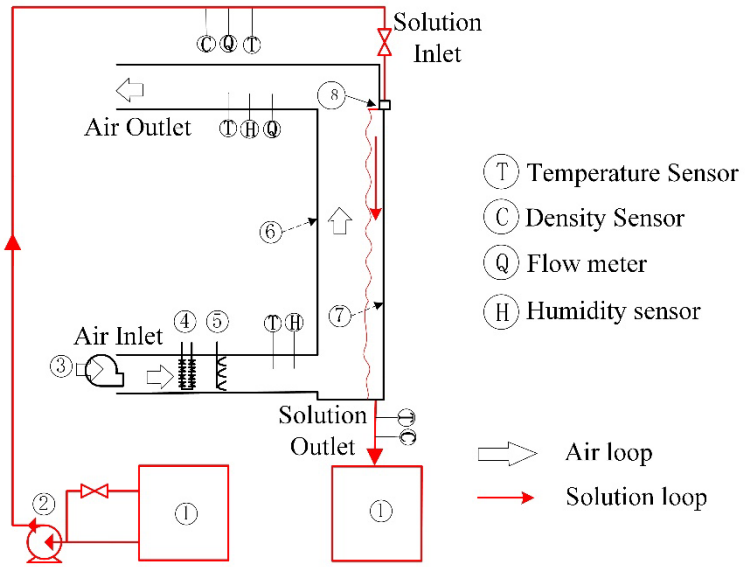

1、Solution tanks 2、Solution pump 3、Air fan 4、Air heater 5、Humidifier
6、Air channel 7、Working surface 8、Solution distributor

Fig. 3. Schematic diagram of the experimental system.

3.2 Configuration of computational model

The schematic diagram of the single channel falling film dehumidifier is illustrated at the left side of Fig. 4. During the experiments, it was found the falling film was nearly eudipleural. Therefore, in order to reduce the calculation amount, the computational domain was only half of the actual dehumidifier, as shown in Fig. 4. The detailed dimension of the computational domain is 250 mm*30 mm*540 mm (Length*Width*Height). The software of ICEM was used to get structured mesh for the domain and part of the mesh is illustrated in Fig. 4. As one can see, in order to capture the flow behavior of the thin liquid desiccant falling film, the size of the mesh was very small near the plate and then becomes greater and greater gradually to reduce the computational time.

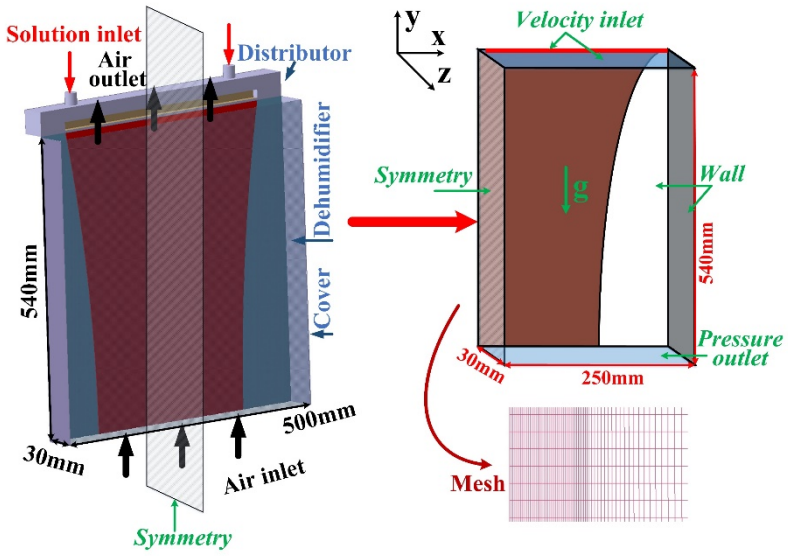

Fig. 4. Sketch map of the dehumidifier and computational domain.

3.3 Boundary conditions, initial and calculation settings

In present study, the commercial CFD software Fluent was used to simulate the simultaneous heat and mass transfer during dehumidification. The boundary conditions for different parts in the computational domain is shown in Fig. 4. The left side was set as symmetry and the right side was set as adiabatic wall. The front side and back side of the physical model were all set as wall. The whole bottom was regarded as pressure outlet. The top side was divided into two parts, namely liquid desiccant inlet and processed air outlet (counter flow was arranged in the dehumidifier). The boundaries for these two parts both were velocity inlet. As the processed air outflowed from the top side, the magnitude of air velocity was set as negative value during simulation.

At the beginning of the simulation, the processed air occupied the whole computational domain which corresponded to the air volume fraction α_g of 1 and liquid desiccant volume fraction α_l of 0 at $t=0$. The inlet humidity and temperature of the moist air and inlet concentration and temperature of liquid desiccant were given at the interface of the Fluent software. As the effect of gravity was taken into consideration in present study, the body force weighted pressure discretization scheme was adopted during simulation [26]. In order to decouple the pressure and velocity equations, the SIMPLE (Semi-Implicit Method for Pressure Linked Equations) along with the highly recommended PRESTO! pressure interpolation scheme [45] was used. The first order upwind scheme was applied to solve the momentum, turbulence, energy and species transport equations. To judge

whether the steady state was achieved or not, the average air humidity at the gas outlet was monitored.

4 Model validation

4.1 Grid independence validation

ICEM software was used to obtain structured mesh for the computational domain. During simulation, the liquid desiccant falling film flowed along the plate dehumidifier with a pretty thin film thickness (usually less than 1mm). In order to capture the flow characteristics of the thin film, fine size grid with the width less than 0.1mm was applied for the domain near the wall, as indicated in Fig 4. Generally, the computational accuracy increases with the increase of mesh quality. However, the increase of mesh quality not only increase the computational accuracy but also computational cost at the same time. Therefore, there exists a balance between the computational accuracy and cost. Therefore, to reduce the computational time, less mesh quality is desired if the computational accuracy is desirable. Therefore, the study of grid independence validation is conducted before simulation. The grid structures for grid independence validation were initially selected according to the study of Luo et al. [38] on 2D simulation. According to their results and the ratio of structural parameters between our model and theirs, five different levels of grid structure with the size of 41×221×601 (Width×Length×Height), 56×221×601, 102×371×1001, 102×520×1402 and 152×371×1001 were selected for comparison. It is also worth mentioning that the size in the width direction was arranged to make sure it was thin enough to accurately capture the thin falling film. The simulation conditions for solution side included the LiCl concentration and temperature of 38% and 28^{o}C respectively and the inlet velocity of 0.12m/s. For air side, the absolute humidity content and temperature of air were 20g/kg and 27^{o}C and the inlet air velocity was 0.6 m/s. As the result for grid independence validation was only affected by the mesh quality but seldom affected by the magnitude of contact angle, a contact angle of 50^{o} was selected for an example. Absolute moisture removal, which is defined by the difference of humidity content between the inlet and outlet air, was selected to evaluate the dehumidification performance. The absolute moisture

removals under different grid structures were compared in Fig. 5. It is clear that the absolute moisture removal firstly increased with the increasing of mesh quality and then levelled off at the grid structure of 102*371*1001. As a result, to keep a balance between the simulation accuracy and computational time, the subsequent simulation chose this grid structure for further study.

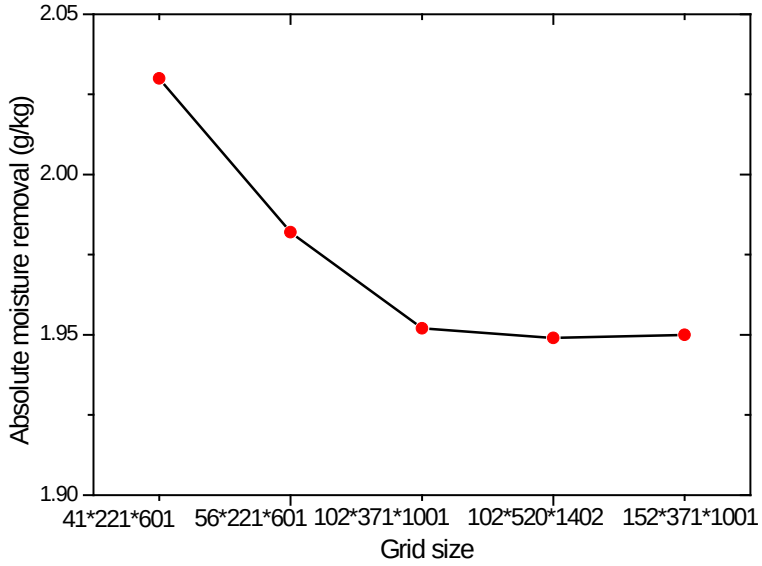

Fig. 5. Absolute moisture removal at different grid sizes.

4.2 Validation of developed 3D model by mass transfer performance

The newly developed 3D simulation model based on CFD technology was validated in terms of mass transfer performance. Experiments were conducted by the abovementioned experimental system shown in Fig. 3. The detailed operating conditions were listed out in Table 1. Similarly, simulations were carried out based on the developed 3D model under the conditions shown in Table 1. As the contact angle of LiCl solution has significant effect on the wettability of falling film on dehumidifier, the contact angle of LiCl solution on the stainless steel was purposely measured by a standard contact angle goniometer with an accurcay of 0.1^{o}, and the result of 58.5^{o} is presented in Fig. 6. Accordingly, the contact angle in the CFD setting panel was also set as 58.5^{o} to reflect the actual wettability of dehumidifier. The comparison results between the experimental absolute moisture removal and numerical ones are shown in Fig. 7. It is clear that the absolute moisture removal increases with the increasing of inlet humidity content for both experiment and simulation. Moreover, the values for the experimental and calculated ones are also

agreed well with each other. For example, when the inlet humidity content is 21g/kg, the absolute moisture removal is 1.95g/kg for experiment and 1.9g/kg for simulation. The greatest difference occurs at the humidity content of 17g/kg. However, the experiment and simulation results are 1.17g/kg and 1.39g/kg with a difference of only 0.22g/kg. Consequently, the novel 3D simulation model can predict the dehumidification performance accurately, which provides an effective way to investigate the effects of different factors on dehumidification performance quantitatively.

Table. 1. Working conditions for the experiments and simulations.

Parameter	$u_s(m/s)$	$X_s(\%)$	$T_s(^oC)$	$u_a(kg/s)$	$d_{a,i}(g/kg)$	$T_a(^oC)$
Magnitude	0.12	35	27	0.7	21	27

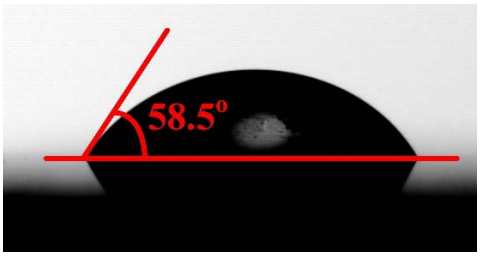

Fig. 6. Contact angles of LiCl solution.

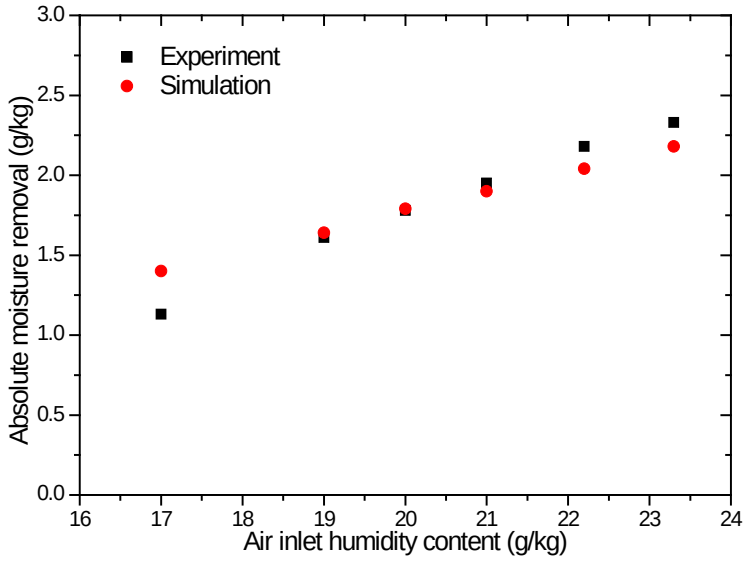

Fig. 7. Comparison between the measured and simulated absolute moisture removal.

5 Parametric study on dehumidification performance

The parametric study is to identify the influences of different parameters on dehumidification performance in the practical application. In the real operation of the liquid desiccant system, dehumidification process is adopted to deal with the latent

load in the processed air. Therefore, the temperature, humidity and velocity of processed air will affect the performance of a dehumidifier. As liquid desiccant, LiCl solution for example, is the solution for water vapor absorption, its temperature, concentration and velocity will also have effect on the mass transfer process. The contact angle can reflect the wettability of material of the dehumidifier and directly affect the heat and mass transfer contact area. Therefore, it also has significant effect on the dehumidification performance. To systematically investigate different parameters on dehumidification performance, the abovementioned parameters are included in the parametric study.

5.1 Influence of air temperature

By adopting the validated 3D CFD model, the influences of various parameters on dehumidification performance were studied. Fig. 8 indicates the absolute moisture removals under different air temperatures. The surface contact angle was set as 50°. As shown, the absolute moisture removals keep constant at the value of 2.1g/kg even though the air temperature varies from 24°C to 36°C. The explanation is that the change of air temperature has little effect on the wettability and mass transfer coefficient during dehumidification process. The wetting area was kept at 0.152m^2. The mass transfer coefficient was determined by Equations (12)-(15). As the change of air temperature in present study had negligible influence on the diffusion coefficient of D_g, the whole mass transfer coefficient would have negligible change under different air temperatures.

As the falling film shrunk gradually along the flow direction, the dehumidification processes at different y-z planes are different. To analyze the influence of falling film shrinkage on mass transfer behavior, the contours of water vapor at y-z planes with different x values are compared in Fig. 9. It is obvious that the distribution of humidity content at different y-z planes is different. It is noteworthy that the water vapor volume friction at y-z plane with x=0.1m shows the lowest value, which corresponds to best dehumidification performance. According to Fig. 9, the falling film (the blue part in Fig. 9) fully wetted the dehumidifier in the

planes of x=0m and x=0.05m. And the falling film in y-z plane with x=0.1m almost fully wetted the plate with only a small non-wetted area at the bottom. However, the falling film did not fully wet the planes with x=0.15m and x=0.2m with a large proportional of non-wetted area. Due to the longer contact time of processed air with solution, more water vapor was absorbed by liquid desiccant and the water vapor volume fractions in the planes with x=0m, x=0.05m and x=0.1m were lower than that of the other two planes correspondingly. Moreover, as shown in the dotted box and the corresponding local enlarged drawing, there existed a falling film boundary in the y-z plane of x=0.1m. In this area, the turbulence of flow was vigorous which corresponded to intense heat and mass transfer with the processed air. The intense dehumidification process could be demonstrated by the dramatical change of contours in this zone. Consequently, more water vapor was absorbed and led to lower water vapor volume fraction in the y-z plane with x=0.1m. However, the 2D simulation can only reflect the heat and mass transfer behavior of one y-z plane. Therefore, it is necessary to develop the 3D model to explore the detailed dehumidification behavior in an actual dehumidifier. Moreover, the falling film lengths at x-z planes with different y values are indicated and compared in Fig. 10. As shown, the falling film consists of main part with nearly uniform film thickness and a rim part with a bulge. Along the flowing direction, the length of the falling film becomes smaller and smaller, which means that the falling film shrinks gradually. Therefore, the water vapor absorption by LiCl solution only occurs on the wetted area in the 3D model. However, in a 2D model, as the film shrinkage can not be simulated, it assumes that the absorption happens on the whole plate dehumidifier which is not practical.

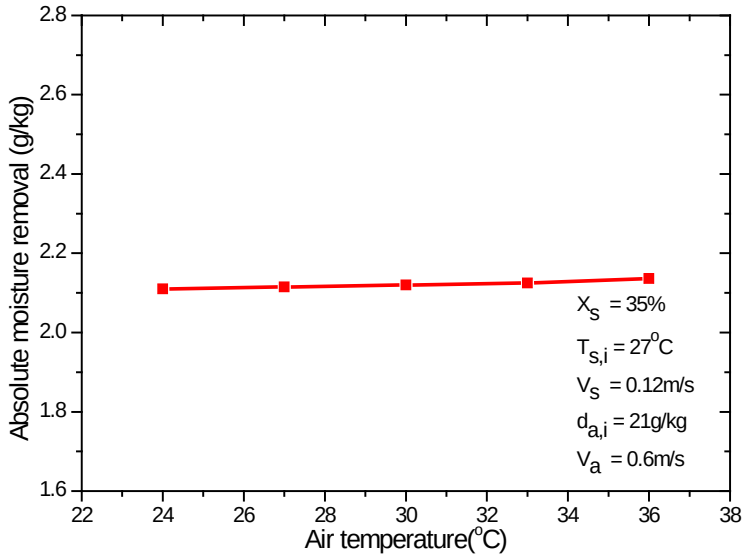

Fig. 8. Influence of air temperature on dehumidification performance.

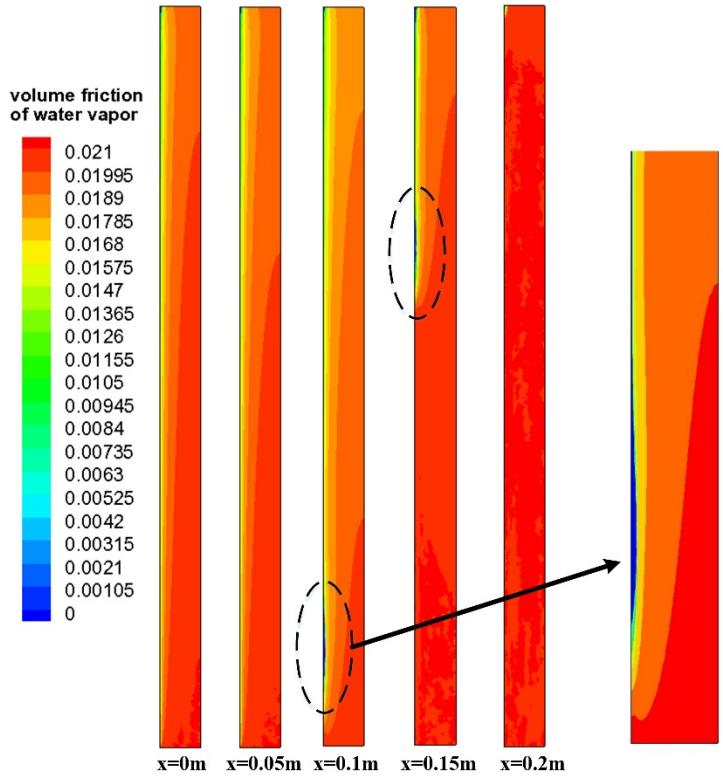

Fig. 9. Contour of water vapor at different y-z plane.

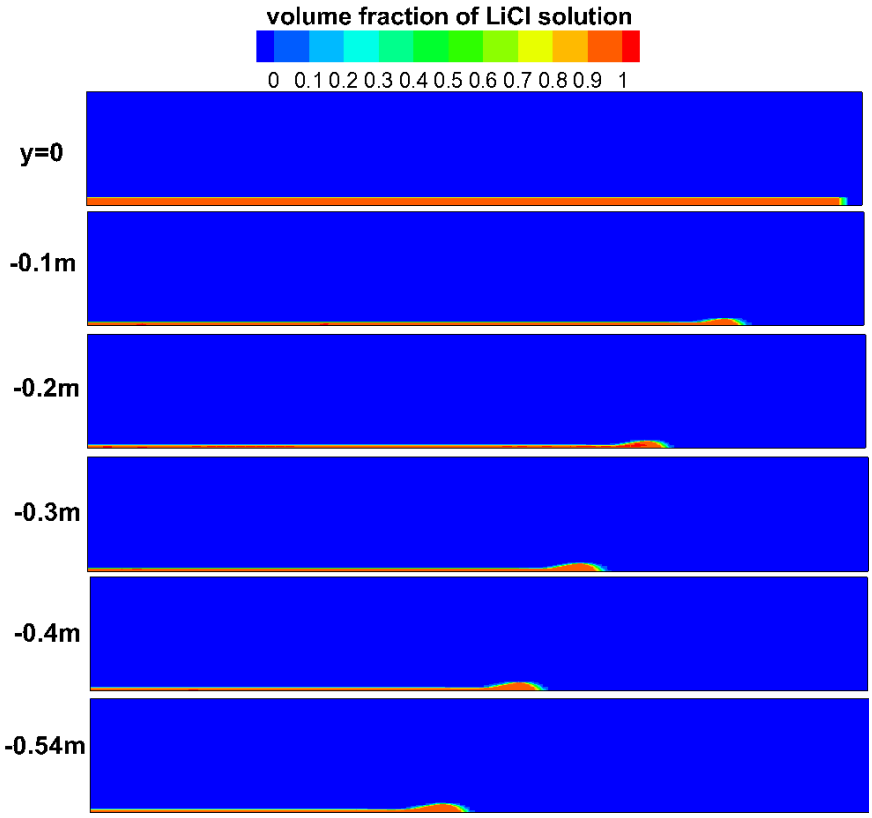

Fig. 10. Contour of LiCl solution at different x-z planes.

5.2 Influence of air velocity

The influence of air flow rate on absolute moisture removal is illustrated in Fig. 11. Under the operational conditions shown in Fig. 11 and surface contact angle of 50^{o}, when the air velocity increases from 0.2m/s to 1.2m/s, the corresponding absolute moisture removal shows a reduction of 2.35g/kg from 3.77g/kg to 1.42g/kg. The contours of moisture content at the air outlet are compared in Fig. 12. It is clear that the humidity content tends to be smaller near the falling film and becomes greater gradually. Moreover, the water vapor gradient is more distinct at lower air velocity, which indicates that more water vapor was absorbed by LiCl solution and better dehumidification performance was obtained. The main reason is that lower air velocity corresponds to longer contact time between processed air and LiCl solution, which is also indicated in Fig. 11. As can be seen, the change tendencies of absolute moisture removal and contact time are similar with each other.

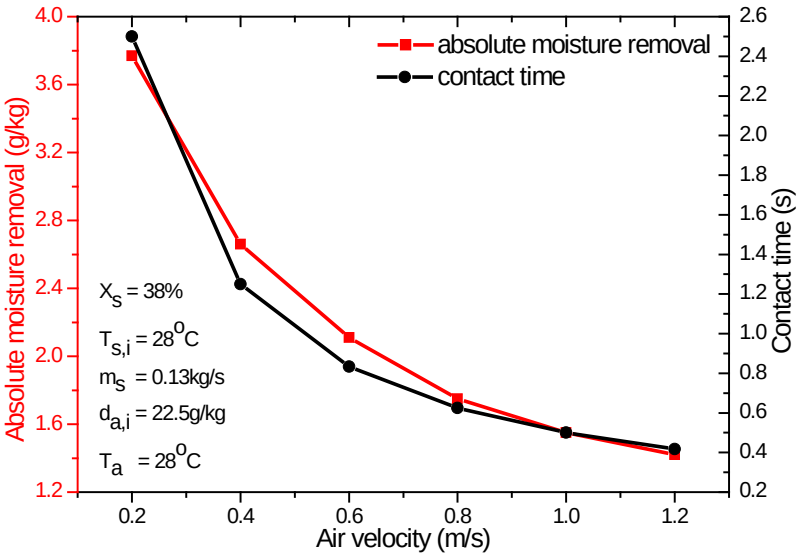

Fig. 11. Influence of air velocity on dehumidification performance.

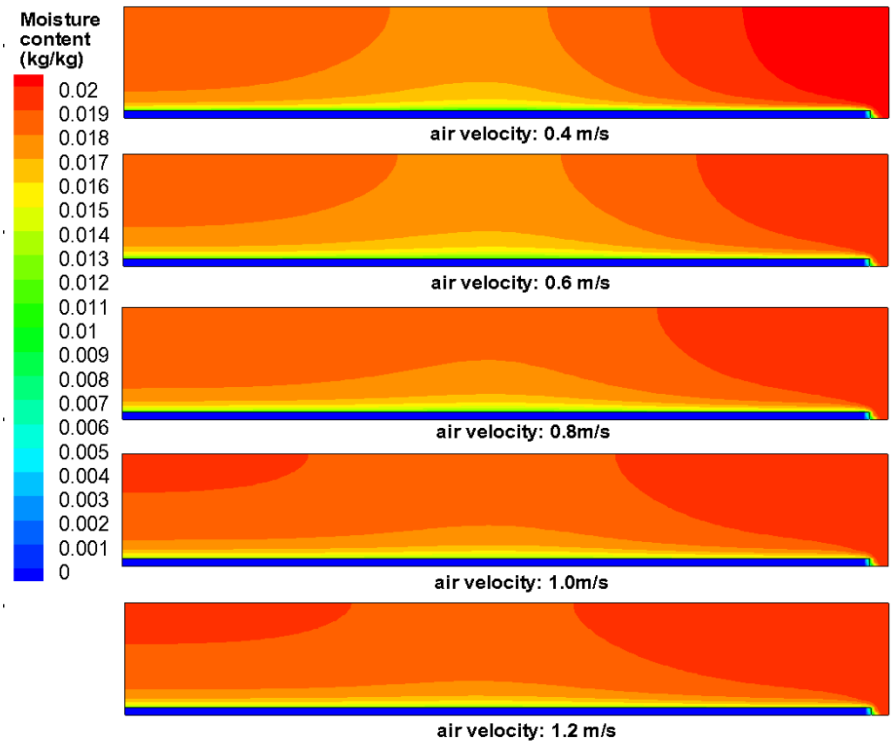

Fig. 12. Contour of moisture content under different air velocities at air outlet.

5.3 Influence of air humidity

Fig. 13 shows the absolute moisture removals at different inlet air humidity. The absolute moisture removal almost shows a liner increment with the increase of air inlet humidity. Specifically, the absolute moisture removal increases from 0.95g/kg to 2.41g/kg when the air inlet humidity increases from 13g/kg to 23g/kg, which is caused by the increment of mass transfer driving force shown in Equation (16). The

mass transfer driving force in terms of moisture content difference between process air and LiCl solution has an increment of 10g/kg from 6.53g/kg to 16.53g/kg correspondingly. What is more, the comparison of contours of moisture content at the same x-z plane with y=-10mm was given under the inlet humidity content of 15g/kg and 21kg/kg, as shown in Fig. 14. As mentioned before, the moisture content changes significantly near the solution falling film. However, in the zone far from the falling film, the moisture content still maintains high. For example, when the inlet humidity content is 15g/kg, the moisture content near the outlet is still lager than 13g/kg at most of the zone. Similar results can be also observed in Fig. 14 for the inlet air humidity of 21g/kg. This indicates that near the falling film, when the moisture content different between the solution and processed air is great, intensive absorption occurs which results in the low moisture content of processed air near the falling film. However, in the air zone far from the falling film, water vapor transfers driven by moisture content difference in the form of diffusion. The key point is that the diffusion coefficient of water vapor in air is quite small, which is the reason of the high humidity content in most of the air zone.

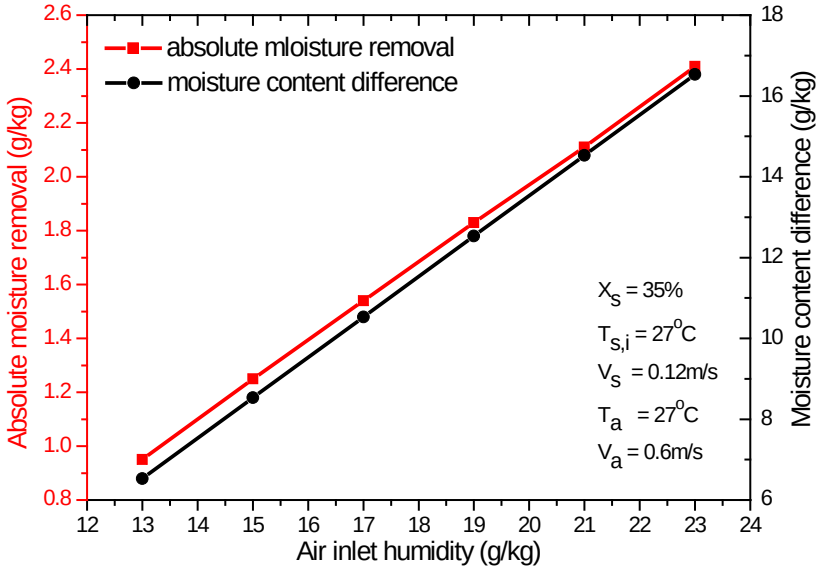

Fig. 13. Influence of air inlet humidity on dehumidification performance.

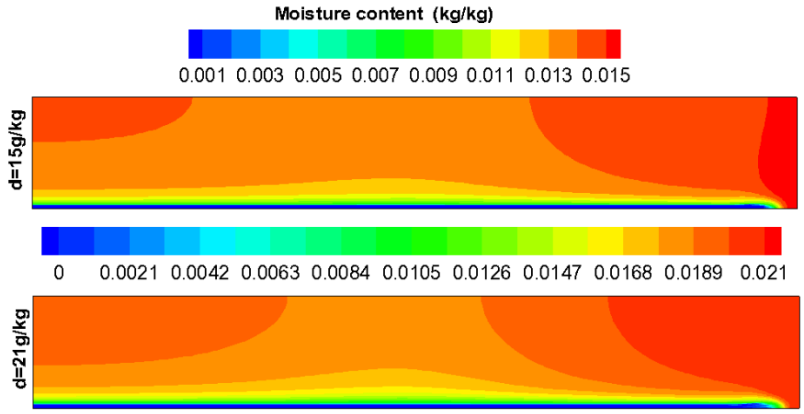

Fig. 14. Comparison of moisture content contours at the x-z plane with y=-10mm under different inlet humidity.

5.4 Influence of solution inlet velocity

As shown in Fig. 15, the absolute moisture removals under various solution inlet velocities are compared. When the solution inlet velocity increases from 0.08m/s to 0.18m/s, the absolute moisture removal increases from 1.63g/kg to 2.3g/kg gradually which is partially caused by the increase of wetting area. As shown in Fig. 15, the actual wetting area has an increment of 0.027m^2 from 0.138m^2 to 0.165m^2. The detailed distributions of solution falling films on plate dehumidifier at various solution velocities can be found in Fig. 16. However, the relative increment of wetting area is 19.6% which is smaller than that of the absolute increment of 41.1%. Therefore, the mass transfer improvement is also resulted from the increment of mass transfer coefficient. Obtained from Equation (15), the increment of solution inlet velocity will lead to the increment of solution superficial velocity u_{surf} and decrement of contact time t_c. As a result, the whole mass transfer coefficient will be greater at higher solution inlet velocity.

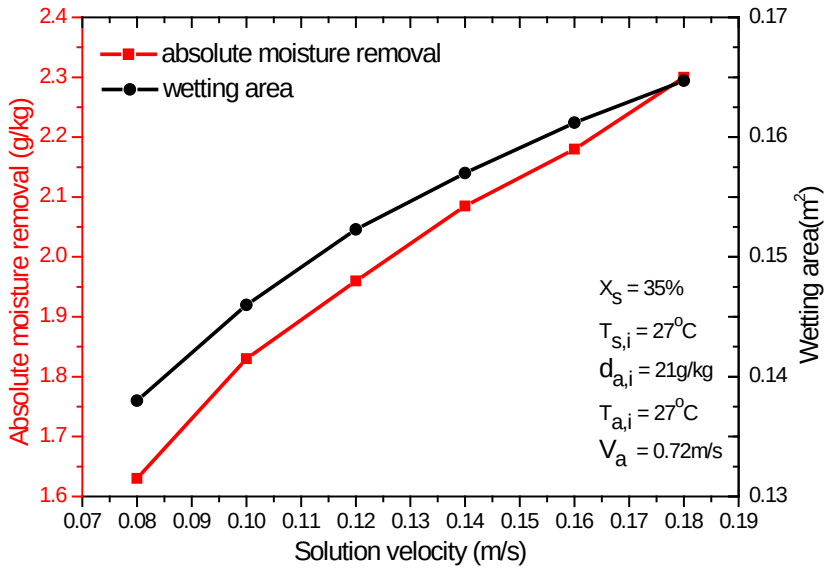

Fig. 15. Influence of solution velocity on dehumidification performance.

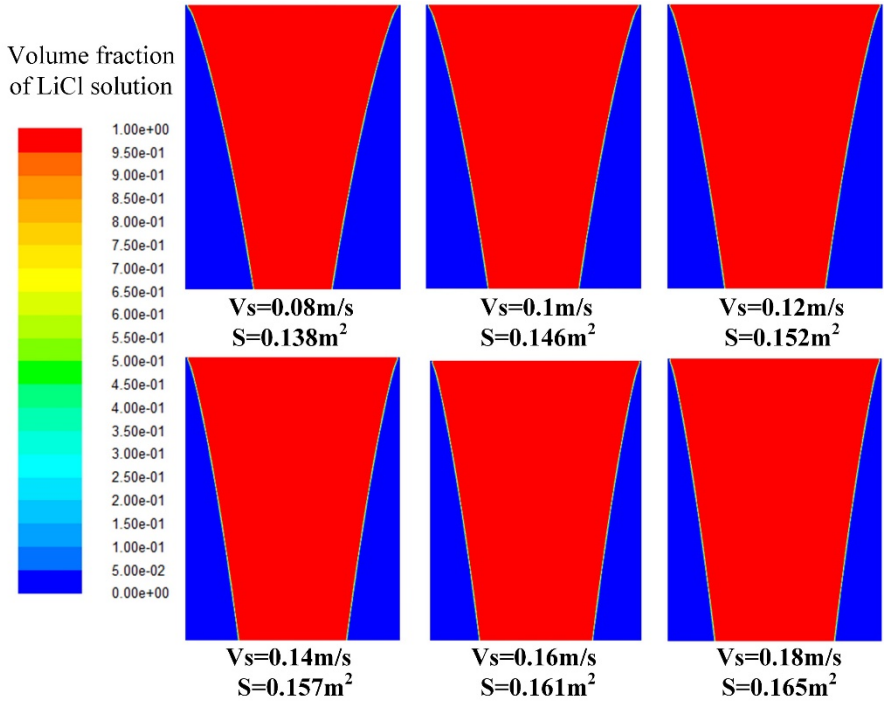

Fig. 16. Comparison of wettability of falling film under different solution flow rates.

5.5 Influence of solution temperature

Fig. 17 illustrates the dehumidification performance in terms of absolute moisture removal at different solution temperatures. Obviously, the absolute moisture removal presents a distinct decrement with the increment of solution temperature. Specially, the value shows a decrement of 0.84g/kg from 2.54g/kg to 1.7g/kg when solution temperature increases from 18° to 33°. The increase of solution temperature leads to the increment of solution vapor pressure and decrement of mass transfer driving force

with moisture content decreasing from 17.4g/kg to 11.62g/kg, which is the contributor of absolute moisture removal decrement. In fact, the local mass transfer coefficients between LiCl falling film and processed air at x-z plane (y=-0.25m) are compared in Fig. 18. It is noteworthy that as the dehumidification process only occurred at the phase interface between processed air and solution, the contours in Fig. 18 were just the phase interface with the LiCl solution volume friction of 0.01~0.99. Under the solution temperatures of 21°C, 27°C and 33°C, the local average mass transfer coefficient maintains around the value of 0.520kg/(m^2.s) with pretty small fluctuations. That is to say, the change of solution temperature has negligible influence on the mass transfer coefficient. As a result, the relative reduction of absolute moisture removal with the value of 49.4% is almost the same with that of the relative decrement of moisture content difference with the value of 49.7%.

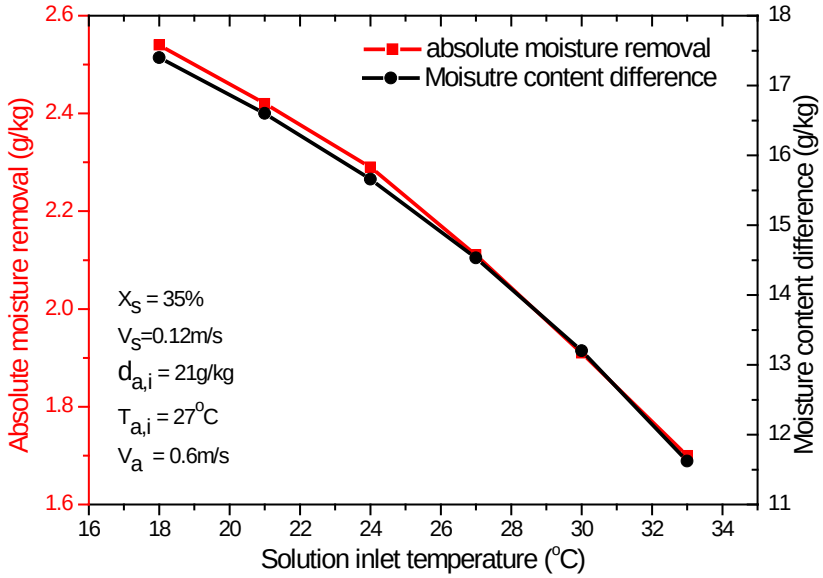

Fig. 17. Influence of solution inlet temperature on dehumidification performance.

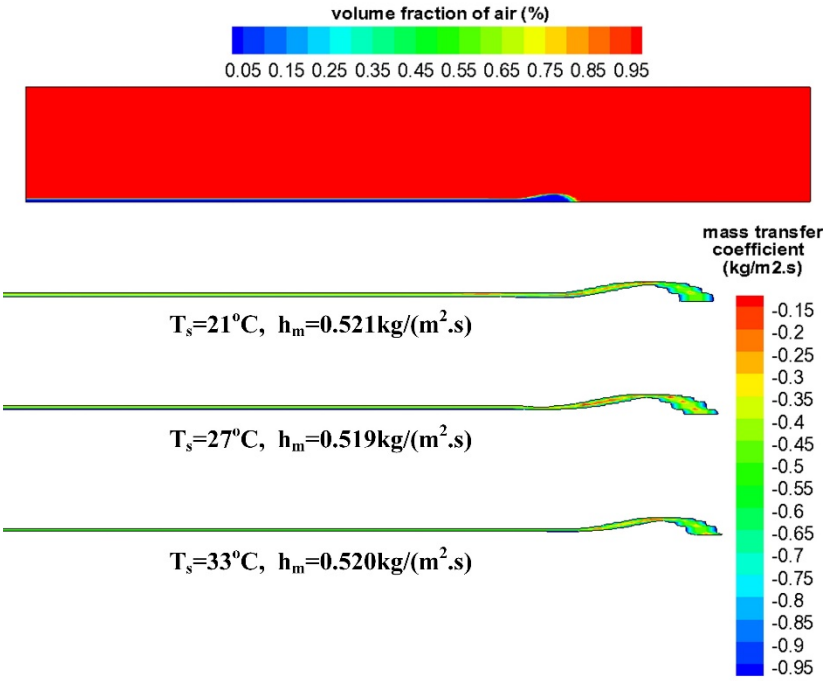

Fig. 18. Contours of mass transfer coefficient under different solution temperatures at y=-250mm.

5.6 Influence of solution concentration

The effect of solution concentration on dehumidification performance is presented in Fig. 19. Due to the increment of mass transfer driving force in terms of moisture content difference, the absolute moisture removal increases from 1.8g/kg to 2.38g/kg when the solution concentration changes from 31% to 39%. In Fig. 20, the mass friction of LiCl at the outlet falling film (only the solution zone is presented in Fig. 20) is illustrated under different inlet solution concentrations. It is clear that the LiCl concentration shows the smallest value at the phase interface and then gradually increases to the stable value which is the same with that of the inlet concentration. Moreover, the thickness of the falling film with detectable concentration change is pretty small, as can be demonstrated in Fig. 20. In other words, the water vapor absorption occurs at the phase interface firstly and leads to the LiCl concentration decrement at the surface of the falling film. In the falling film, the LiCl transfer in solution is driven by the concentration difference between the phase/gas interface and main part of falling film. However, such transfer proceeds mainly in the form of diffusion as the turbulence in the falling film is small. As a result, the solution concentration is pretty low at the falling film surface but almost maintains at the inlet concentration at other parts of the falling film.

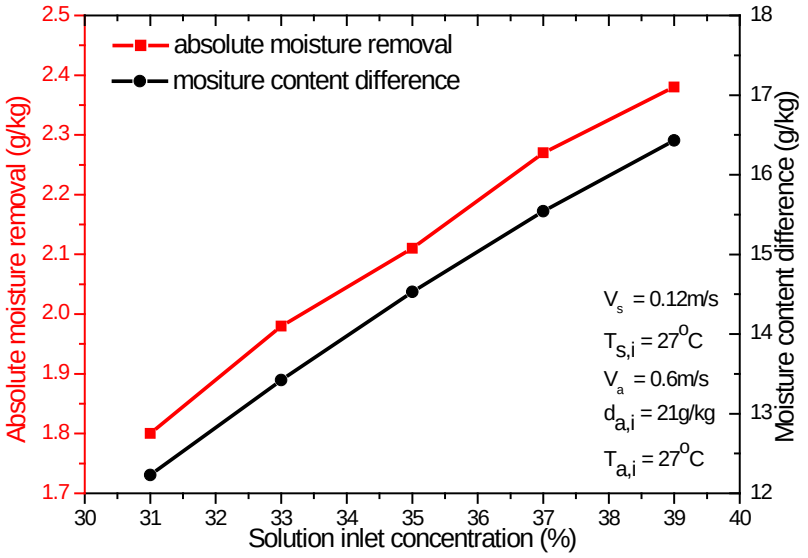

Fig. 19. Influence of solution inlet concentration on dehumidification performance.

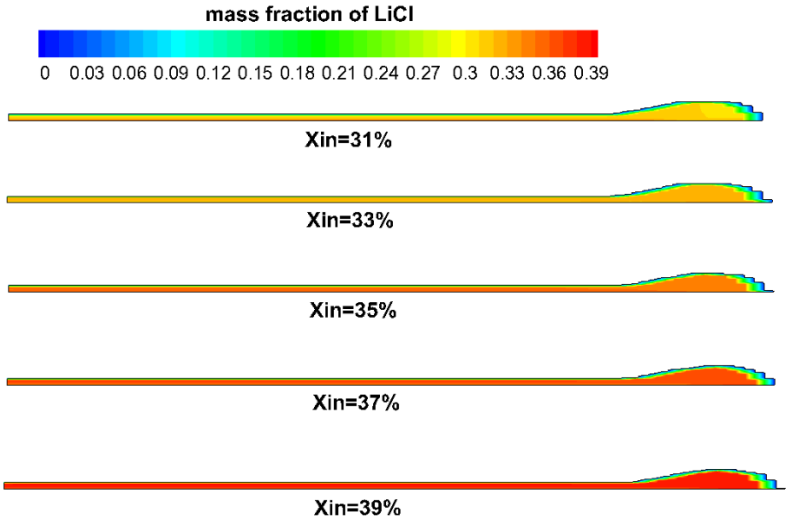

Fig. 20. Mass fraction of LiCl at the solution outlet.

5.7 Influence of surface contact angle

As different materials with different wettability may be adopted for the fabrication of dehumidifiers, the contact angles of LiCl solution on these materials may be different. Therefore, the absolute moisture removals under different surface contact angles are simulated and compared in Fig. 21 to indicate the influence of surface wettability. Apparently, the absolute moisture removal presents a significant decrement with the increment of contact angle. Specifically speaking, when the contact angle increases from 10^o to 90^o, the absolute moisture removal decreases from 2.36g/kg to 1.6g/kg. The solution contact angle on the dehumidifier is a crucial parameter to determine the wettability of the falling film on the plate. Under the

operational conditions shown in Fig. 21, the wetting area of falling film on dehumidifier decreases from 0.21m^2 to 0.091m^2 when the contact angle changes from 10^o to 90^o, as shown in Fig. 22. In fact, the relative decrement of absolute moisture content is smaller that of the wetting area. Such seemed discrepancy is caused because the decrement of falling film wetting area leads to the increment of solution velocity as the solution flow rate is constant. According to Equations (12) to (15), the increment of solution velocity will result in the increase of mass transfer coefficient. Finally, as the relative decrement of wetting area is greater than that of the relative increment of mass transfer coefficient, the absolute moisture removal shows a declining tendency, as shown in Fig. 21.

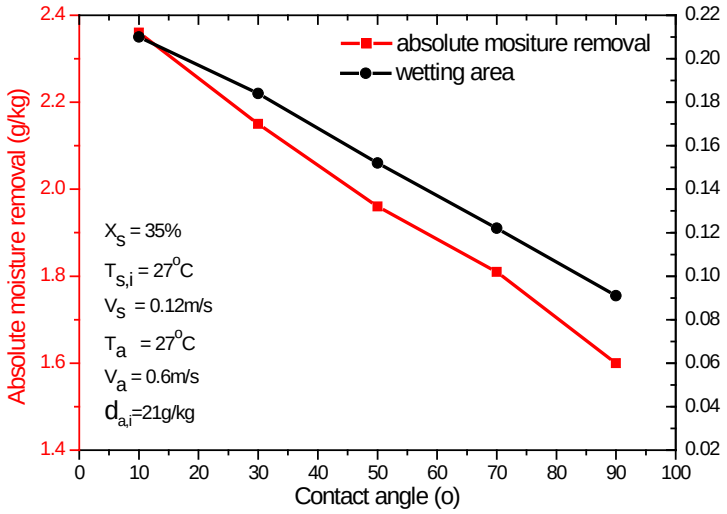

Fig. 21. Humidity variation along the x direction.

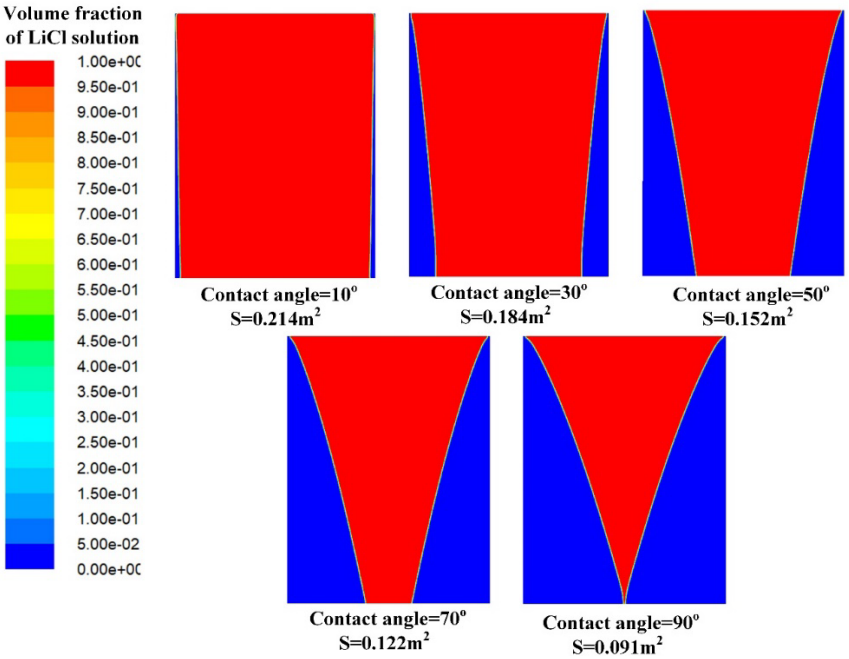

Fig. 22. Wettability of falling film at different contact angles.

5.8 Discussion on the simulation results

The effects of various operational parameters on mass transfer performance were compared and analyzed in Fig. 8 to 22. As the change of air temperature has negligible influences on both wettability and mass transfer driving force, it has nearly no effect on mass transfer performance. Differently, the air humidity, solution temperature and concentration are directly related with the mass transfer driving force, their change can always affect the dehumidification performance significantly. The wettability of falling film on dehumidifier increases with the increasing of solution flow rate and decreases with the increasing of contact angle. The change of wettability directly influences the behavior of mass transfer during dehumidifier. For the influence of air velocity, its increase leads to the decrement of absolute moisture change due to the decrease of contact time between solution and processed air.

Based on the 3D simulation, it is clear that as the falling film shrinks along the flow direction, the dehumidification process occurred in the dehumidifier is inhomogeneous, as demonstrated in Fig. 9. However, both the film shrinkage and inhomogeneous mass transfer process can not be described by 2D simulation, which clearly indicates the necessity of 3D simulation. Moreover, as shown in Fig. 12 and Fig. 20, the intensive mass transfer process mainly occurs at the phase interface,

which results in the sharp change of both humidity content and solution concentration. However, in the flow zone away from the phase interface, water vapor transfer in processed air or LiCl transfer in solution proceeds mainly in the form of diffusion. Due to the low diffusion coefficients, such kind of mass transfer greatly reduces the dehumidification performance, which could be indirectly verified by the high vapor humidity content or solution concentration far from the phase interface.

Based on the simulation results on the detailed dehumidification behavior, some practical suggestions to improve the dehumidification performance are put forward as follows: firstly, some dehumidifiers with modified structures, such as plate-fin structure and curved plate, could be adopted to replace the plane plate. Such structures can improve the flow turbulence in both falling film and processed air to increase the mixing of fluids. The increment of turbulence in flow can lead to strong mass exchange in solution or air and thus quicken the mass transfer rate and dehumidification performance. Then, as indicted in Fig. 21 and Fig. 22, the contact angle plays a vital role in determining the falling film wettability and dehumidification performance. Consequently, specific super-hydrophilic coating can be pasted on the surface of the dehumidifier for greater wetting area and better dehumidification performance. For example, by adopting the super-hydrophilic nano titanium dioxide (TiO_2) coating developed by our research group, the contact angle can be reduced from 58.5^o to 14^o, as shown in Fig. 23. It is noteworthy that the present study mainly focuses on developing and validating the newly proposed 3D model. Therefore, the detailed investigations on suggested dehumidification enhancement approaches are not carried out temporarily. In our future study, more elaborative studies on such aspects will be conducted on the basis of the developed 3D model.

Fig. 23. Contact angle of LiCl solution on stainless steel dehumidifier with coating.

6 Conclusion

A novel 3D simulation model based on CFD technology was developed to study

the dehumidification performance of a falling film dehumidifier. After validation by the experimental data, the newly proposed 3D model was used to explore the simultaneous hydrodynamics and dehumidification process in the dehumidifier. Some of the conclusive remarks were drawn and presented as follows:

(1) Due to the falling film shrinkage on the dehumidifier, the flow and dehumidification behavior in the dehumidifier was inhomogeneous, which could not be reflected by 2D simulation model.

(2) The parameter, i.e. inlet air humidity, solution temperature and concentration directly, determined the mass transfer driving force with distinct impact on dehumidification performance. The absolute moisture removal almost kept constant at different air temperatures but increased with the increase of air velocity. For solution flow velocity, greater flow velocity corresponded to larger wetting area and better dehumidification performance as well.

(3) Intense water vapor absorption occurred at the phase interface, which led to great concentration gradient of both solution and humidity contents near the falling film interface. However, mass transfer in the zone away from the interface mainly proceeded in the form of diffusion, which left nearly unchanged solution concentration and relatively high humidity content in such zone. Therefore, some modified dehumidifier structures, such as plate-fin and curved plate, could be employed to improve the turbulence in fluid flow for the purpose of dehumidification enhancement.

(4) The 3D simulation was able to evaluate the influence of contact angle on dehumidification performance. Smaller contact angles corresponded to better wettability of falling film and dehumidification performance as well. Therefore, from the prospect of contact angle, the super-hydrophilic coating could be applied on the dehumidifier surface to improve the wettability for better dehumidification performance.

The novel 3D CFD simulation model is a promising and economic approach to study the detailed heat and mass transfer behavior not only in the liquid desiccant cooling system but also in other relevant fields, such as absorption refrigerant,

evaporative cooling and chemical absorption. The simulation results can give detailed information on mass transfer characteristic and thus provide some basic guidance for the design and operation of dehumidifier. However, the present study mainly focused on the validation of model and parametric study of difference influencing factors, which has limited direct contribution for the practical application of the liquid desiccant cooling system. Besides, we only focused on the dehumidification process and paid little attention on regeneration process which is another indispensable process in the system. Therefore, in the future study, further studies will be conducted to investigate the effects of different configurations of dehumidifiers on mass transfer. Moreover, new 3D CFD simulation model will also be developed for regeneration process to study the detailed heat and mass transfer behavior.

Acknowledgement

The work is financially supported by Hong Kong Research Grant Council through General Research Fund (PolyU 152010/15E and PolyU 152184/17E).

References

[1] Nicol JF, Humphreys MA. Adaptive thermal comfort and sustainable thermal standards for buildings. Energy and buildings. 2002;34:563-72.

[2] Nicol F. Adaptive thermal comfort standards in the hot–humid tropics. Energy and buildings. 2004;36:628-37.

[3] She X, Cong L, Nie B, Leng G, Peng H, Chen Y, et al. Energy-efficient and-economic technologies for air conditioning with vapor compression refrigeration: A comprehensive review. Applied Energy. 2018;232:157-86.

[4] Qi R, Lu L, Yang H. Development of simplified prediction model for internally cooled/heated liquid desiccant dehumidification system. Energy and buildings. 2013;59:133-42.

[5] Ge G, Xiao F, Niu X. Control strategies for a liquid desiccant air-conditioning system. Energy and buildings. 2011;43:1499-507.

[6] Wen T, Zhan H, Zhang D, Lu L. Development of evaporation pressure-capacity control strategy for aircraft vapor cycle system. International Journal of Refrigeration. 2017;83:14-22.

[7] Luo Y, Yang H, Lu L. Dynamic and microscopic simulation of the counter-current flow in a liquid desiccant dehumidifier. Applied Energy. 2014;136:1018-25.

[8] Luo Y, Wang M, Yang H, Lu L, Peng J. Experimental study of internally cooled liquid desiccant dehumidification: application in Hong Kong and intensive analysis of influencing factors. Building and Environment. 2015;93:210-20.

[9] Grossman G, Johannsen A. Solar cooling and air conditioning. Progress in Energy and Combustion

Science. 1981;7:185-228.
[10] Zhang L-Z, Zelik EB. Total heat recovery: heat and moisture recovery from ventilation air: Nova Science Publ.; 2008.
[11] Islam M, Alan S, Chua K. Studying the heat and mass transfer process of liquid desiccant for dehumidification and cooling. Applied Energy. 2018;221:334-47.
[12] Ou X, Cai W, He X, Zhai D. Experimental investigations on heat and mass transfer performances of a liquid desiccant cooling and dehumidification system. Applied Energy. 2018;220:164-75.
[13] Wan KK, Li DH, Liu D, Lam JC. Future trends of building heating and cooling loads and energy consumption in different climates. Building and Environment. 2011;46:223-34.
[14] Wen T, Lu L, Zhong H. Investigation on the dehumidification performance of LiCl/H2O-MWNTs nanofluid in a falling film dehumidifier. Building and Environment. 2018;139:8-16.
[15] Wen T, Lu L, Yang H, Luo Y. Investigation on the Regeneration and Corrosion Characteristics of an Anodized Aluminum Plate Regenerator. Energies. 2018;11:1-15.
[16] Wen T, Lu L, Dong C, Luo Y. Development and experimental study of a novel plate dehumidifier made of anodized aluminum. Energy. 2018;144:169-77.
[17] Wen T, Lu L, Dong C. Enhancing the dehumidification performance of LiCl solution with surfactant PVP-K30. Energy and Buildings. 2018;171:183-95.
[18] Luo Y, Yang H, Lu L, Qi R. A review of the mathematical models for predicting the heat and mass transfer process in the liquid desiccant dehumidifier. Renewable and Sustainable Energy Reviews. 2014;31:587-99.
[19] Dong C, Lu L, Wen T. Experimental study on dehumidification performance enhancement by TiO2 superhydrophilic coating for liquid desiccant plate dehumidifiers. Building and Environment. 2017;124:219-31.
[20] Wen T, Lu L. Numerical and experimental study on internally cooled liquid desiccant dehumidification concerning film shrinkage shape and vapor condensation. International Journal of Thermal Sciences. 2019;136:316-27.
[21] Wen T, Luo Y, He W, Gang W, Sheng L. Development of a novel quasi-3D model to investigate the performance of a falling film dehumidifier with CFD technology. International Journal of Heat and Mass Transfer. 2019;132:431-42.
[22] Yadav AS, Bhagoria J. Heat transfer and fluid flow analysis of solar air heater: a review of CFD approach. Renewable and Sustainable Energy Reviews. 2013;23:60-79.
[23] Norton T, Sun D-W. Computational fluid dynamics (CFD)–an effective and efficient design and analysis tool for the food industry: a review. Trends in Food Science & Technology. 2006;17:600-20.
[24] Bhutta MMA, Hayat N, Bashir MH, Khan AR, Ahmad KN, Khan S. CFD applications in various heat exchangers design: A review. Applied Thermal Engineering. 2012;32:1-12.
[25] Min JK, Park IS. Numerical study for laminar wavy motions of liquid film flow on vertical wall. International Journal of Heat and Mass Transfer. 2011;54:3256-66.
[26] Gu F, Liu CJ, Yuan XG, Yu GC. CFD simulation of liquid film flow on inclined plates. Chemical engineering & technology. 2004;27:1099-104.
[27] Szulczewska B, Zbicinski I, Gorak A. Liquid flow on structured packing: CFD simulation and experimental study. Chemical engineering & technology. 2003;26:580-4.
[28] Ho C-D, Chang H, Chen H-J, Chang C-L, Li H-H, Chang Y-Y. CFD simulation of the two-phase flow for a falling film microreactor. International Journal of Heat and Mass Transfer. 2011;54:3740-8.
[29] Subramanian K, Wozny G. Analysis of hydrodynamics of fluid flow on corrugated sheets of packing.

International Journal of Chemical Engineering. 2012;2012.
[30] Xu Y, Yuan J, Repke J-U, Wozny G. CFD study on liquid flow behavior on inclined flat plate focusing on effect of flow rate. Engineering Applications of Computational Fluid Mechanics. 2012;6:186-94.
[31] Banerjee R. A numerical study of combined heat and mass transfer in an inclined channel using the VOF multiphase model. Numerical Heat Transfer, Part A: Applications. 2007;52:163-83.
[32] Bo S, Ma X, Chen H, Lan Z. Numerical simulation on vapor absorption by wavy lithium bromide aqueous solution films. Heat and mass transfer. 2011;47:1611.
[33] Kharangate CR, Lee H, Mudawar I. Computational modeling of turbulent evaporating falling films. International Journal of Heat and Mass Transfer. 2015;81:52-62.
[34] Bo S, Ma X, Lan Z, Chen J, Chen H. Numerical simulation on the falling film absorption process in a counter-flow absorber. Chemical Engineering Journal. 2010;156:607-12.
[35] Hu J, Yang X, Yu J, Dai G. Carbon dioxide (CO2) absorption and interfacial mass transfer across vertically confined free liquid film-a numerical investigation. Chemical Engineering and Processing: Process Intensification. 2017;111:46-56.
[36] Haelssig JB, Tremblay AY, Thibault J, Etemad SG. Direct numerical simulation of interphase heat and mass transfer in multicomponent vapour–liquid flows. International Journal of Heat and Mass Transfer. 2010;53:3947-60.
[37] Luo Y, Yang H, Lu L. Liquid desiccant dehumidifier: Development of a new performance predication model based on CFD. International Journal of Heat and Mass Transfer. 2014;69:408-16.
[38] Luo Y, Chen Y, Yang H, Wang Y. Study on an internally-cooled liquid desiccant dehumidifier with CFD model. Applied energy. 2017;194:399-409.
[39] Luo Y, Shao S, Xu H, Tian C, Yang H. Experimental and theoretical research of a fin-tube type internally-cooled liquid desiccant dehumidifier. Applied Energy. 2014;133:127-34.
[40] Wen T, Lu L, Dong C, Luo Y. Investigation on the regeneration performance of liquid desiccant by adding surfactant PVP-K30. International Journal of Heat and Mass Transfer. 2018;123:445-54.
[41] Wen T, Lu L, Zhong H, Dong C. Experimental and numerical study on the regeneration performance of LiCl solution with surfactant and nanoparticles. International Journal of Heat and Mass Transfer. 2018;127:154-64.
[42] Dong C, Lu L, Qi R. Model development of heat/mass transfer for internally cooled dehumidifier concerning liquid film shrinkage shape and contact angles. Building and Environment. 2017;114:11-22.
[43] Haghshenas Fard M, Zivdar M, Rahimi R, Nasr Esfahani M, Afacan A, Nandakumar K, et al. CFD simulation of mass transfer efficiency and pressure drop in a structured packed distillation column. Chemical engineering & technology. 2007;30:854-61.
[44] Banerjee R, Isaac K. Evaluation of turbulence closure schemes for stratified two phase flow. ASME 2003 International Mechanical Engineering Congress and Exposition: American Society of Mechanical Engineers; 2003. p. 689-705.
[45] Fluent I. Fluent 6.3 Users Guide (2006). Google Scholar.
[46] Bird RB. Transport phenomena. Applied Mechanics Reviews. 2002;55:R1-R4.
[47] Zhang L, Hihara E, Matsuoka F, Dang C. Experimental analysis of mass transfer in adiabatic structured packing dehumidifier/regenerator with liquid desiccant. International Journal of Heat and Mass Transfer. 2010;53:2856-63.
[48] Lowenstein A, Gabruk R. Effect of absorber design on the performance of a liquid-desiccant air conditioner. ASHRAE Winter Meeting, Anaheim, CA, USA, 01/25-29/921992. p. 712-20.